Journal of Electroceramics 4:S1, 81–90, 1999
© 2000 Kluwer Academic Publishers, Boston. Manufactured in The Netherlands.

Niobium Doping Effect on Resistivity of Epitaxially Grown Nb-$SrTiO_3$ Thin Films by Laser Ablation Method

K. FUKUSHIMA & S. SHIBAGAKI
Advanced Technology Research Laboratories, Sumitomo Metal Industries, LTD., 1 Nishino Cho, Higashimukoujima, Amagasaki, Hyogo, 660-0891, Japan

Submitted November 14, 1997; Revised December 21, 1998; January 5, 1999

Abstract. Thin films of Nb doped $SrTiO_x$ (Nb-STO) have been fabricated on $SrTiO_3$ (100) substrates by the pulsed laser deposition (PLD) technique. The effect of the oxygen pressure and the substrate temperature on film properties such as surface roughness, lattice constants and film compositions has been investigated. The preferential orientation of Nb-STO films was *a*-axis at the substrate temperature of 400°C ~ 700°C and at the oxygen pressures lower than 3×10^{-1} Torr. At the low oxygen pressure, the Nb-STO film grew in the two dimensional mode. The surface morphology was strongly affected by the oxygen pressure. Both the lattice constant of the *a*-axis and Nb contents in the Nb-STO films increased as the oxygen pressure decreased, while they were hardly affected by the change in the substrate temperature. Furthermore, the electrical properties of Nb-STO films were also influenced by oxygen pressure and by valence of the Nb ion.

Keywords: $SrTiO_3$, PLD, laser ablation, Nb doped $SrTiO_x$

1. Introduction

Strontium titanate ($SrTiO_3$) is well known as a typical dielectric material and as an attractive material for its variable properties such as electrical transport, optical absorption, and structural phase transitions. Recently, $SrTiO_3$ has been used as a suitable substrate for growth of various oxide thin films like High Tc superconducting thin films [1]. Furthermore, many researchers have also tried to fabricate $SrTiO_3$ thin films for application to electrical devices [2]. $SrTiO_3$ thin films with good crystallinity and variable conductivity will enable us to design some remarkable devices, for example, multi-layers thin films such as semiconductor/insulator/semiconductor (S/I/S) junctions and metal/insulator/metal (M/I/M) junctions. In the case of bulk $SrTiO_3$, it is known to be changed in its electrical properties by reduction treatments [3] or by doping [4]. In order to obtain $SrTiO_3$ thin films with controllable conductivity, it is necessary to clarify the origin of the electrical properties, such as the oxygen deficiency in films and substitution of cations.

In this paper, we focused on the film properties such as lattice constant and composition of epitaxial Nb-doped $SrTiO_x$ (Nb-STO) thin films deposited by the pulsed laser deposition (PLD) technique. We also tried to construct multi-layer structures with epitaxial (Nb-)STO thin films.

2. Experimental

A schematic diagram of our apparatus for PLD is shown in Fig. 1. An ArF excimer laser (wave length 193 nm, pulse width 20 nsec) was operated at a repetition rate of 5 Hz. The laser was introduced with an incidence angle of 30° relative to the target through the UV grade fused silica window. The laser fluence on the target surface was estimated to be about 4 J/cm^2 in an irradiation area of 4×10^{-2} cm^2. The distance between substrate and target was 4.5 cm. A Nb 0.5 wt % $SrTiO_3$ target was prepared by doping Nb atoms into a $SrTiO_3$ single crystal. In order to avoid local heating of the target surface, it was rotated at ~ 2 rpm during the laser ablation. The substrate was a

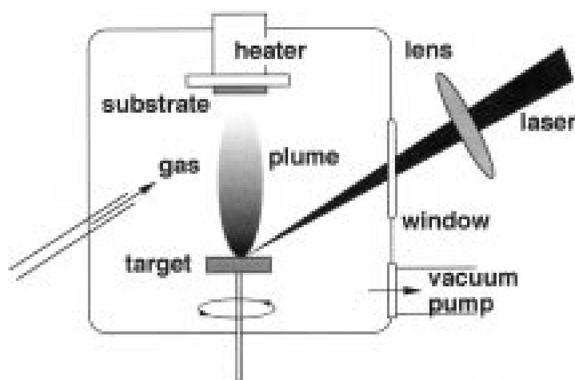

Fig. 1. A schematic diagram of the growth chamber for laser ablation.

$SrTiO_3$ (100) single crystal polished by conventional methods. The substrate temperature was changed from 400°C to 700°C. The O_2 pressure in our deposition chamber was controlled by evacuating with a turbomolecular pump, and was varied from 3×10^{-4} Torr to 3×10^{-1} Torr. The deposition conditions are listed in Table 1. The crystallinity of Nb-STO films was examined by X-ray diffraction (XRD). The microstructure and the surface morphology of films were investigated by transmission electron microscopy (TEM) and atomic force microscopy (AFM), respectively. The film composition was estimated by secondary ion mass spectroscopy (SIMS), comparing with standard samples which were Nb_ySrTiO_3 single crystals $(0.05\,\text{wt}\,\% \leqq y \leqq 0.5\,\text{wt}\,\%)$. The valences of these thin films were measured by X-ray photoelectron spectroscopy (XPS; VG Scientific: VG-Microlab 320-D) method using Mg K α as the X-ray source, and all spectra were referenced to the adventitious C 1s peak at 285.0 eV. Because the concentration of Nb was lower than that of Sr, Ti and O, the integration time for the Nb 3d spectrum was multiplied by 16 compared to those of Sr, Ti and O.

Table 1. Growth condition of Nb-STO thin films by PLD

Substrate	$SrTiO_3$ (100)
Target	$Nb_{0.5wt\%}SrTiO_3$
Laser beam	ArF excimer laser
Substrate temperature	400°C ~ 700°C
Laser power	~ 4J/cm^2, 5 Hz
Oxygen pressure	3×10^{-4} Torr ~ 3×10^{-1} Torr
Film thickness	~ 400

3. Results and Discussion

3.1. Film Properties

3.1.1. Crystallinity and lattice constant. Figure 2 shows the XRD patterns of the $SrTiO_3$ (STO) substrate and the Nb-STO films deposited at the substrate temperature of 650°C and oxygen pressures from 3×10^{-4} Torr to 3×10^{-1} Torr. The patterns of Nb-STO films deposited at 650°C showed (h00) peaks only, which meant that the Nb-STO films were purely *a*-axis oriented films. In the case of films deposited at oxygen pressures lower than 1.4×10^{-2} Torr, small peaks originating from Nb-STO (100) reflections were observed close to the STO (100) peak in XRD patterns. Furthermore, the peak position of (100) was shifted to higher angles 2θ as the oxygen pressure increased. This indicated that *a*-axis lattice constant of Nb-STO thin films became larger as the oxygen pressure decreased.

Figure 3 shows the XRD patterns of Nb-STO films deposited at the various substrate temperatures. All the diffraction patterns consisted of peaks from STO substrates and peaks assigned as (h00) reflections of Nb-STO films. All the diffraction angles of peaks from Nb-STO films were hardly changed as the substrate temperature increased. From the Nb-STO peak angles, the lattice constants were estimated. Figure 4 shows the lattice constant, *a*-axis, of the Nb-STO films as a function of (a) oxygen pressure and (b) substrate temperature. Increasing the oxygen pressure from 3×10^{-4} Torr up to 3×10^{-1} Torr, the lattice constant decreased from 4.005 to 3.905. At oxygen pressures higher than $\sim 3 \times 10^{-1}$ Torr, the lattice constant of the films seemed to approach that of a $SrTiO_3$ single crystal. On the other hand, the lattice constant did not depend on the substrate temperature. They were larger than that of a $SrTiO_3$ single crystal, which were 3.99 ± 0.025Å.

The change in lattice constant of (Nb-)STO thin films has been observed by some researchers. Tomio et al. observed that the lattice constant of Nb-STO films were extended due to the substitution of Nb for Ti atoms by laser ablation of the various Nb-composition targets, $SrTi_{1-x}Nb_xO_3$ [2]. It was also reported that the lattice constant of $SrTiO_3$ films depended on the composition ratio of $Sr/(Sr + Ti)$ which was varied by the insertion of excess SrO between SrO and TiO_2 planes [5]. In our case, however, it was expected that the variation of the

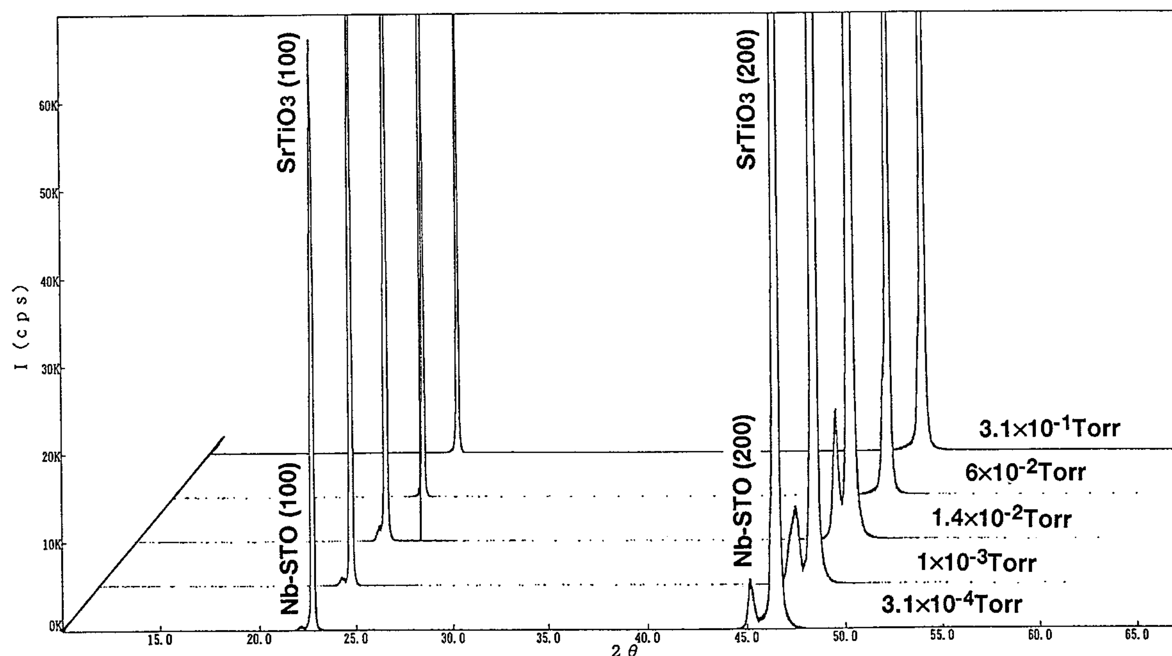

Fig. 2. X-ray diffraction patterns of the Nb doped $SrTiO_x$ films (Nb-STO) deposited at the oxygen pressure from 3×10^{-4} Torr to 3.1×10^{-1} Torr. All films were deposited at the substrate temperature of 650°C.

lattice constant was not only due to the difference in the cation ratio but possibly due to the oxygen content (deficiency) of the Nb-STO films. The oxygen deficiency in the films was enhanced under lower oxygen pressures. Since the lack of O^{2-} in TiO_2 or SrO planes may increase the Coulomb repulsive force between those planes, the lattice constant could be extended as the oxygen pressure decreased. In fact, it has been observed that the lattice constant of bulk $SrTiO_3$ was enlarged when the partial oxygen pressure was very low during annealing treatments at high temperatures [6]. However, the lattice constant of Nb-STO films as shown in Fig. 4(a) was larger than the value estimated from the ideal oxygen deficiency in bulk $SrTiO_3$.

3.1.2. Surface morphology. Figure 5 shows the AFM images of the surface of Nb-STO films with thickness of around 40 nm. At the oxygen pressure of 3×10^{-1} Torr, the film surface consisted of small grains or crystallites of several tens nm size. This suggested that Nb-STO films grew in a two-dimensional mode at the low oxygen pressures (high vacuum). The variation of growth mode from the two-dimensional mode into the three-dimensional mode with increasing oxygen pressure could be related to the change in kinetic energy of impinging atoms on the substrate during film growth. In the laser ablation process, it is well known that the kinetic energy of ablation atoms decreases as the atmospheric pressure increases [7] and a part of the kinetic energy changes into the migration energy of atoms on a substrate surface [8]. Therefore, as the oxygen pressure increased, the available migration energy is expected to decrease. When the migration energy was low, each atom could not sufficiently move around the substrate surface. As a result, a thin film tends to grow three-dimensionally at high oxygen pressures.

At the low oxygen pressure, it was found that the surface morphology of thin films was not influenced by the difference in the substrate temperature during deposition. Figure 6 shows AFM images of the film surfaces of Nb-STO grown at substrate temperatures from 480°C to 700°C. All the Nb-STO films were deposited at the oxygen pressure of 1×10^{-3} Torr. It was observed that the surface morphology of each film was smooth and not very different.

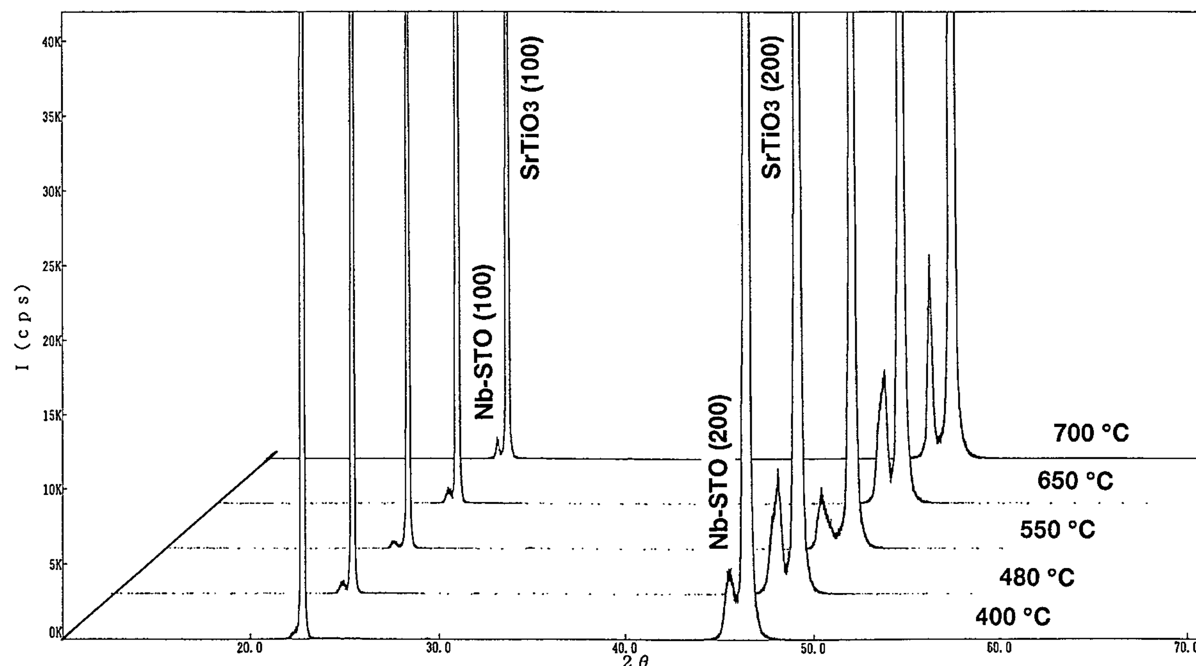

Fig. 3. X-ray diffraction patterns of the Nb doped $SrTiO_x$ films (Nb-STO) deposited at the substrate temperature from 400°C to 700°C. All films were deposited at the oxygen pressure of 1×10^{-3} Torr.

3.1.3. Microstructure. Figure 7 shows a typical cross-sectional TEM image of a Nb-STO thin film. The Nb-STO was an *a*-axis oriented film deposited on a $SrTiO_3$ (100) substrate. Some stacking faults were observed in the Nb-STO film near the substrate surface. However, no other structure or impurity phase could be observed at the interface between the film and the substrate. In the diffraction pattern, it was found that the diffraction spots of (200) and (020) due to the Nb-STO film appeared just on the spots originated from the STO substrate. This means that the Nb-STO grew epitaxially on the STO substrate. According to the diffraction pattern in the figure, the orientational relationship between the Nb-STO film and the STO substrate was found to be [100] film // [100] substrate. Furthermore, we had confirmed that such an epitaxial growth occurred in Nb-STO films deposited at the other conditions.

3.1.4. Film composition. We also investigated Nb contents in Nb-STO films fabricated at the different substrate temperatures and oxygen pressures. Figure 8 shows the atomic ratio of Nb/Ti examined by SIMS as a function of substrate temperatures. It was found that the Nb/Ti ratio in the films was almost the same over a range of substrate temperatures. On the other hand, as the oxygen pressure increased, the Nb/Ti ratios decreased. Though the origin of the change in Nb content is not clear, we believe that the Nb content should relate to the variation of the lattice constant of the Nb-STO films. Remember that the lattice constant of Nb-STO film increased with decreasing oxygen pressure (Fig. 4(a)) at the same time that the Nb contents increased.

3.1.5. Electrical properties. The electrical resistivity of the Nb-STO films was measured by the four-probe method. It was noticed that the resistivity of the Nb-STO films depended on the deposition conditions. Figure 9 shows the temperature dependence of the electrical resistivity of the (Nb-)STO films. The resistivity of Nb-STO film deposited at the oxygen pressure of 2.4×10^{-4} Torr was lower than that of Nb-STO grown at 3.0×10^{-4} Torr. Furthermore, the resistivity of the STO film was larger than that of the Nb-STO film fabricated under

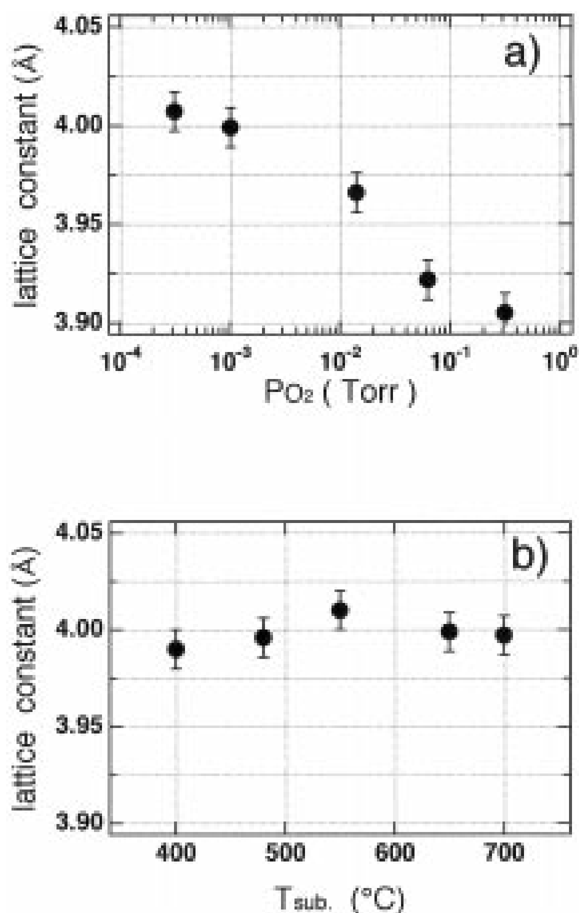

Fig. 4. The lattice constants of *a*-axis of Nb-STO films as a function of (a) the oxygen pressure and (b) the substrate temperature. (a) The substrate temperature was 650°C, and (b) the oxygen pressure was 1×10^{-3} Torr.

the identical condition. Those results suggest that the carrier concentration in Nb-STO thin films was influenced by both the oxygen deficiency and the Nb content. Oxygen deficiency in Nb-STO films causes a deficiency of O_{2-} and results in excess electrons as the electrical carriers. The substitution of Nb^{5+} for Ti^{4+} in $SrTiO_{3-\delta}$ also supplies electrons in Nb-STO films.

In order to elucidate the variation of the resistivity of Nb-STO films, further investigation of the carrier doping mechanism is required. What is the valence of the Nb ions? How about Ti ions in Nb-STO films? What is the coordination of oxygen atoms, or the number of oxygen vacancies? etc.

According to our previous work [9], resistivity of thin films depends on the oxygen pressure. In this experiment (Fig. 9) the resistivity of Nb-STO film deposited at the oxygen pressure of 2.4×10^{-4} Torr was lower than that of Nb-STO grown at 3.0×10^{-4} Torr. This suggests that the oxygen deficiency in the films affected resistivity of the thin films. This effect was also observed in bulk materials [6].

Furthermore, Nb was doped in the thin films in this experiment. The resistivity of the Nb-STO film was about one tenth of that of the STO film. This shows that doping of the Nb ion is also effective for decreasing resistivity. Until now it has been believed that Nb 5+ ion is a source of an electron in the bulk SrTiO$_3$ ceramics. In order to elucidate the role of Nb ion in these thin films, the valence of the Nb ion was measured with XPS (Fig. 10). The substrate temperatures of the three samples were 480, 440, and 550°C, respectively. The sample (a) was a semiconductor and samples (b) and (c) were insulators. In samples (b) and (c) the positions of Nb 3d$_{5/2}$ were both about 207.0 eV. They show that the valence of the Nb ion was 5+. However, in sample (a) the position of 3d$_{5/2}$ shows a chemical shift of about 1.0 eV. According to the literature [10], the binding energy decreases with the decrease of valence. When the valence of a Nb ion is 2+, the binding energy is under 204.7 eV. In this sample, the binding energy is about 206 eV. Therefore, the valence of Nb ion is not +5, probably 4+. The radius of the Nb +5 ion (in an octahedral site) is 0.069 nm and that of the Nb +4 ion (in an octahedral site) is 0.074 nm. Because even the radius of Nb 4+ is smaller than that of Sr 2+ (0.125 nm), the Ti (0.068 nm in an octahedral site) ion is probably substituted with a Nb ion. This substitution distorts the NbO$_6$ octahedron.

In order to clarify the effect of this distortion on the other elements, Sr, Ti, and 0, the valences of these elements were measured. The samples measured here were the same as mentioned in Fig. 10. The measurement revealed that the valences of Sr ions and Ti ions were +2 and +4 in the insulating films and also in the semiconducting film.

In Fig. 11, Ols spectra of the three Nb-SrTiO$_3$ thin films were measured. The samples measured here were the same as those mentioned in Fig. 10. The binding energies of the main peak of Ols are almost the same: 530.2, 529.8, and 530.1 eV, respectively. However, the shapes of the second peak are quite

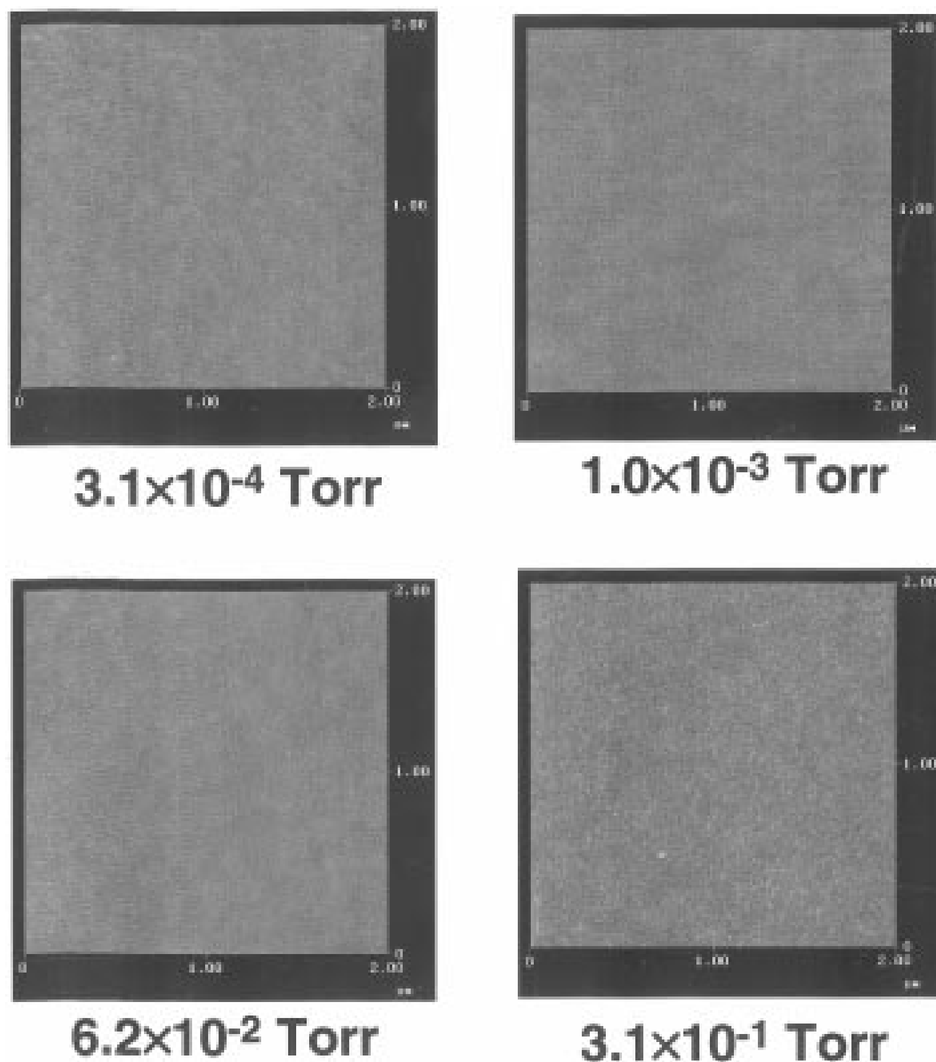

Fig. 5. AFM images of the Nb-STO film surfaces deposited at the oxygen pressure from 3×10^{-4} Torr to 3.1×10^{-1} Torr. All films were deposited at the substrate temperature of 650°C.

different. Because the binding energy of the second peak in the semiconducting film is higher than that in the insulating films, the valence of the O ion in the semiconducting film is a little higher than -2. This change is probably originating from the distortion of the NbO_6 octahedron.

The valence of the Nb ion in the insulating films is $+5$ and the radius of this ion is the same as the radius of the Ti $+4$ ion. Therefore, the NbO_6 octahedron does not distort. However, this octahedron of the Nb $+4$ ion has a large distortion. This distortion changes the valence of the O ion and also desorbs the O ion easily.

This XPS analysis revealed that the presence of Nb decreases resistivity as well as the oxygen vacancy concentration.

3.2. Fabrication of Multi-layer Structures

In order to make novel devices with multi-layer structures, we have tried to synthesize an artificial interface consisting of semiconducting thin film (Nb-

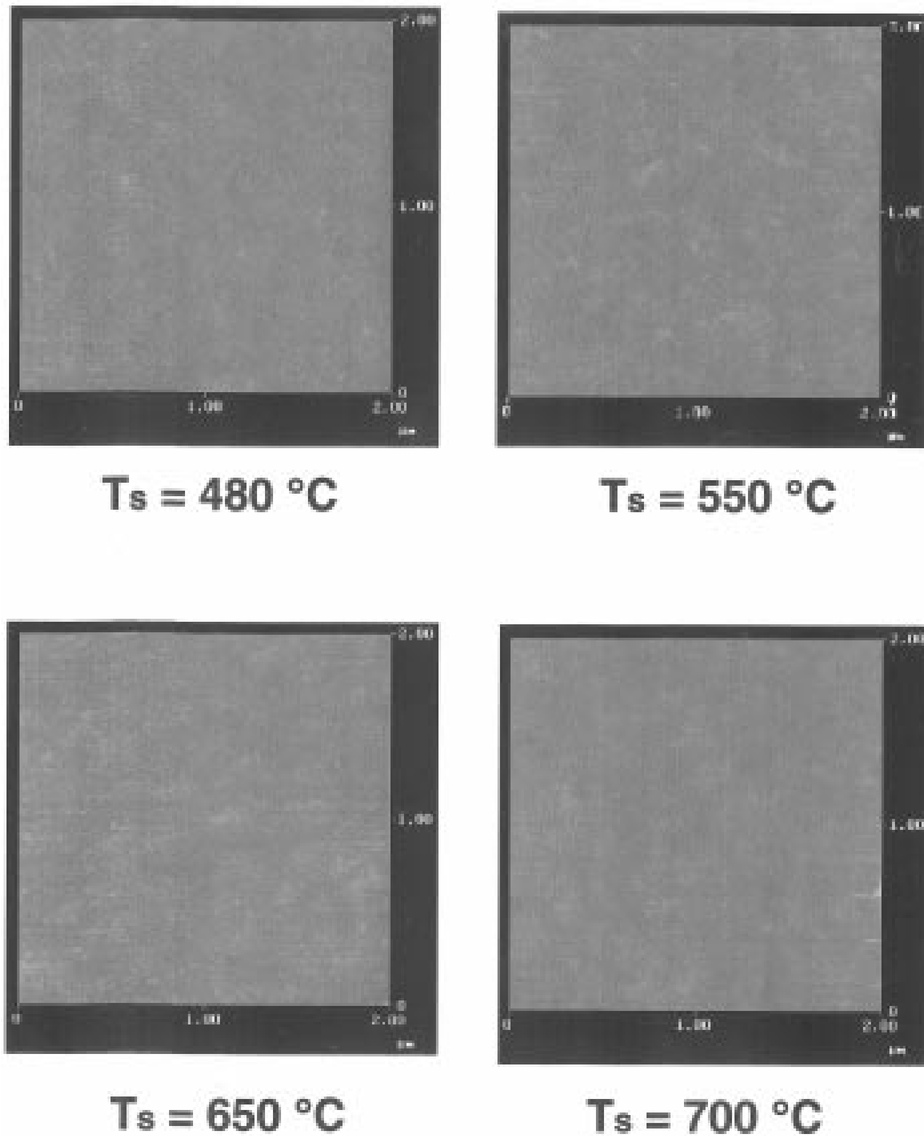

Fig. 6. AFM images of the Nb-STO film surfaces deposited at the substrate temperature from 480°C to 700°C. All films were deposited at the oxygen pressure of 1×10^{-3} Torr.

STO) and insulating thin film (STO), as Nb-STO/STO/Nb-STO/STO substrate. The STO substrate was annealed at 1100°C for 32 h in air to improve its surface morphology. The reason why we chose the annealed STO substrate to fabricate the multi-layer film was as follows. The substrate surface of STO was found to give a step structure by the annealing treatment at high temperatures [9]. The surface morphology with step structures is considered to be effective to judge the film crystallinity grown on it. It is expected that the film surface morphology has the same step structure as the annealed substrate if the deposited thin film epitaxially grows on it. The semiconducting Nb-STO films in the multi-layer structure were deposited on the annealed STO substrate at the oxygen pressure of 3.0×10^{-4} Torr, while the insulating STO film was fabricated on the Nb-STO film at 1.0×10^{-3} Torr and 440°C. The thickness of each layer was around 40 nm. Figure 12 shows the XRD pattern of the multi-layer film. The

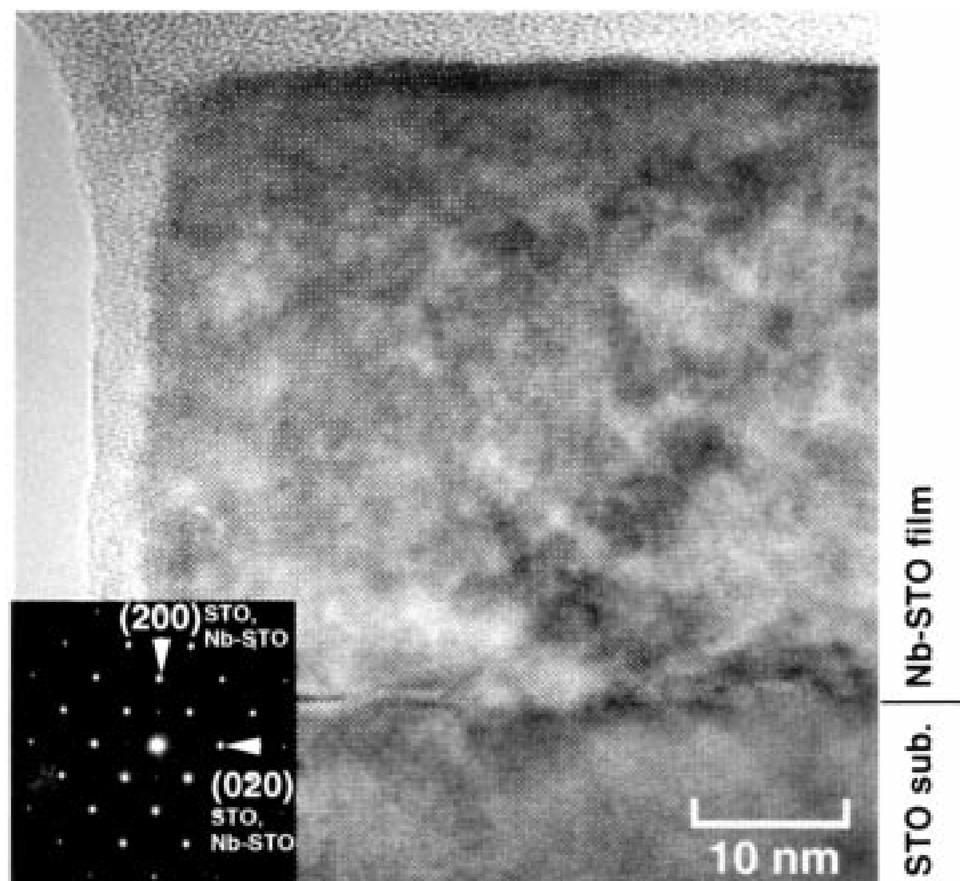

Fig. 7. A typical TEM image of *a*-axis oriented Nb-STO film on a $SrTiO_3(100)$ substrate. Nb-STO film was fabricated at the substrate temperature of 650°C and at the oxygen pressure of 1×10^{-3} Torr. The film thickness was about 40 nm.

diffraction pattern consisted of the STO substrate peak and (200) peak of the multi-layer films. Since there were no other reflections from the (Nb-)STO thin films, each film of the multi-layer structure was considered to be highly oriented to the normal of the growing surfaces. AFM observation of the surface also supported that each layer was epitaxially grown. As shown in Fig. 13, the surface morphology of the multi-layer film had step structures that were observed at the surface of the annealed STO substrate.

4. Summary

We have obtained *a*-axis oriented films of Nb-STO at substrate temperatures of 440°C ~ 700°C and at oxygen pressures from 3×10^{-4} to 3×10^{-1} Torr by means of the PLD technique. It was found that both the oxygen pressure and the substrate temperature affected the film properties of Nb-STO. The *a*-axis lattice constant of the Nb-STO films increased as the oxygen pressure decreased, while it was hardly changed by elevating the substrate temperature. Surface morphology was strongly affected by the oxygen pressure. Furthermore, the electrical properties of these Nb-STO films were also influenced by the oxygen pressure and the valence of the Nb ion. The conductivity of Nb-STO films was increased with decreasing oxygen pressure.

We have also succeeded in fabricating multi-layer structures consisting of semiconducting Nb-STO and insulating STO films. It was found that the topmost

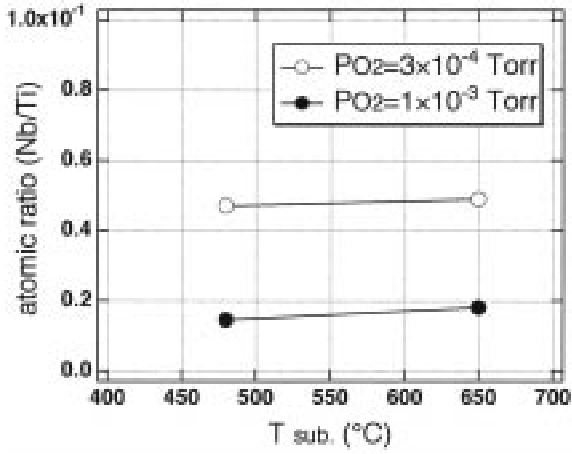

Fig. 8. Dependence of the atomic ratio (Nb/Ti) on the substrate temperature. Nb-STO films were prepared at the oxygen pressure of 3×10^{-4} Torr and 1×10^{-3}, respectively. The ratio was determined by SIMS measurement.

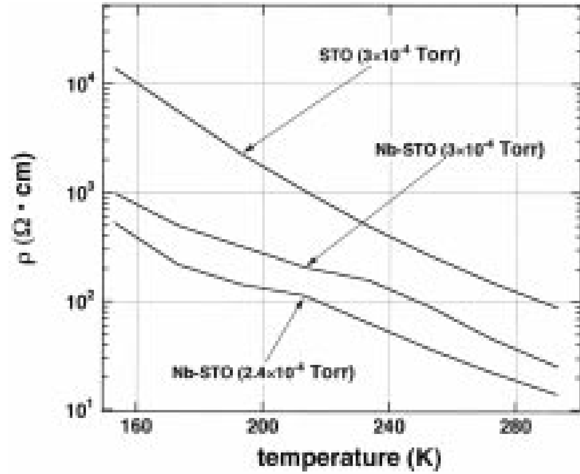

Fig. 9. The temperature dependence of electrical resistivity of Nb-STO films and STO film. Nb-STO films were deposited at the oxygen pressure of 3×10^{-4} Torr and 2.4×10^{-4} Torr, respectively. STO film was deposited at 3×10^{-4} Torr. The substrate temperatures were fixed to 480°C.

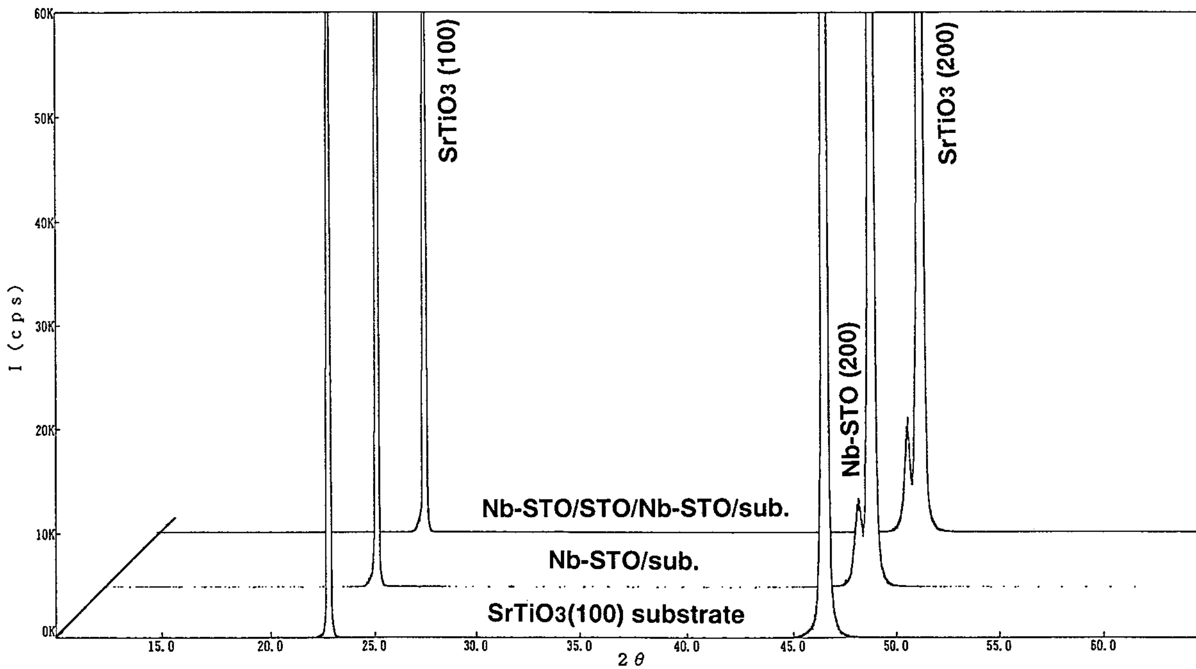

Fig. 10. X-ray diffraction patterns of annealed STO substrate, Nb-STO film deposited on the STO substrate, and the multi-layer film consisted of Nb-STO/STO/Nb-STO/STO substrate. The (200) peak of films appeared near the (200) of STO substrate.

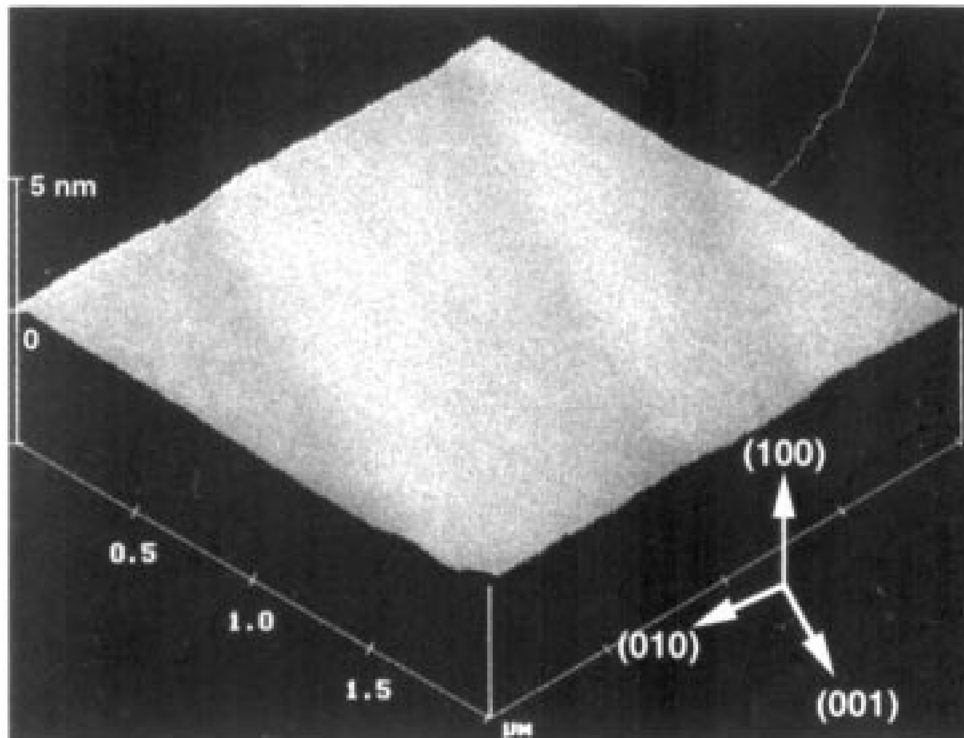

Fig. 11. An AFM image of the surface structure of the multi-layer thin film.

layer of the multi-layer film was either Nb doped TiO_2 planes or SrO planes.

Acknowledgment

We would like to thank Shoichi Naga and Yutaka Ito for their assistance in the observation of AFM and TEM images. This study was performed through Special Coordination Funds of the Science and Technology Agency of the Japanese Government.

References

1. C. W. Chu, P. H. Hor, R. L. Meng, L. Gao, Z. J. Haung, Y. Q. Wang, J. Bechtold, D. Cambel, M.K. Wu, J. Ashburn, and C. Y. Haung, *Phys. Rev. Lett.* **58**, 405 (1987).
2. T. Tomio, H. Miki, H. Tabata, T. Kawai, and S. Kawai, *J. Appl. Phys.* **76**, 5886 (1994).
3. L. C. Walters and R. E. Grace, *J. Phys. Chem. Solids* **28**, 245 (1967).
4. N. Bickel, G. Schmidt, K. Heinz, and K. Müller, *Phys. Rev. Lett.*, **62**, 2009 (1989).
5. H. Yabuta, K. Takemura, H. Yamaguchi, S. Sone, T. Sakuma, and M. Yoshida, *Mat. Res. Soc. Symp. Proc.*, **361**, 325 (1995).
6. S. Shibagaki, A. Hamano, S. Takao, and J. Tanaka, *J. Ceram. Soc. Jpn.*, **102**, 858 (1994).
7. K. Fukushima, Y. Kanke, and T. Morishita, *J. Appl. Phys.*, **74**, 6948 (1993).
8. H. Izumi, K. Ohata, T. Sawada, T. Morishita, and S. Tanaka, *Jpn. J. Appl. Phys.*, **30**, 1956 (1991).
9. K. Fukushima and S. Shibagaki, *Thin Solid Films*, **315**, 238 (1998).
10. Perkin-Elmer Corporation, *Handbook of X-ray Photoelectron Spectroscopy*, 3rd edit. (1987)
11. P. V. Nagakar, P. C. Searson, and F. D. Gealy, *J. Appl. Phys.*, **69(1)**, 459 (1991).